Chapter 4.

Phase Transformations in a

$Cu_{1.6}Mn_{1.4}Al$ Alloy

Phase Transformations in a $Cu_{1.6}Mn_{1.4}Al$ Alloy

Abstract

The phase transformations in the $Cu_{1.6}Mn_{1.4}Al$ alloy have been investigated by means of transmission electron microscopy (TEM) and energy-dispersive X-ray spectrometry (EDS). In as-quenched condition, the microstructure of the alloy was a mixture of ($L2_1$ + B2 + L-J) phases. This is different from that observed by previous workers in the $Cu_{3-x}Mn_xAl$ alloys with X≤1.0. When the as-quenched alloy was aged at 460℃ for short times, γ-brass precipitates started to occur at anti-phase boundaries (APBs). After prolonged aging at 460℃, the γ-brass precipitates grew and β-Mn precipitates were formed at the regions contiguous to the γ-brass precipitates. The coexistence of (γ-brass + β-Mn) has never been observed by previous workers in Cu-Mn-Al alloy systems before.

4-1 Introduction

In previous studies, it is seen that when the $Cu_{3-x}Mn_xAl$ alloys with $0.5 \leqq X \leqq 0.8$ were solution-treated in single β phase (disordered body-centered cubic) region and then quenched rapidly, a β → B2 → ($D0_3$ + $L2_1$) phase transition occurred during quenching [1]; as the Mn content in the $Cu_{3-x}Mn_xAl$ alloy was increased to 25 at.% (X=1), the as-quenched microstructure of the Cu_2MnAl alloy became a single $L2_1$ phase [1-4]. When the $Cu_{3-x}Mn_xAl$ alloys with $0.5 \leqq X \leqq 0.8$ were aged at 300℃ or below for longer times, fine precipitates were observed to appear within the ($D0_3$ + $L2_1$) matrix [1]. The crystal structure of the fine precipitates was determined to be of $L1_0$ having lattice parameters a=0.424 nm, b=0.297 nm and c=0.424 nm [1]. In addition, three kinds of precipitates, namely, γ-brass ($D8_3$), β-Mn (A13) and T-Cu_3Mn_2Al (C15) were reported to form in the Cu_2MnAl alloy after being aged at temperatures ranging from 350℃ to 650℃ [2-6]. It is interesting to note that although the β-Mn precipitate was always found in the aged Cu_2MnAl alloy, we are aware of only one article concerning the orientation relationship between the β-Mn and matrix [4]. In 1987, Kozubski et al. reported that both the morphology of the β-Mn precipitates and the orientation relationship between the β-Mn and $L2_1$ matrix would vary with the aging temperature [4].

Recently, we have performed TEM investigations on the phase transformations of $Cu_{2.2}Mn_{0.8}Al$ and Cu_2MnAl alloys [7-8]. Consequently, we found that the fine precipitates formed in the $Cu_{2.2}Mn_{0.8}Al$ alloy aged at 300℃

should belong to the L-J phase, rather than $L1_0$ phase [7]. The L-J phase has an orthorhombic structure with lattice parameters a = 0.413 nm, b = 0.254 nm and c = 0.728 nm, which was firstly identified by the present workers. In addition, TEM examinations indicated that when the Cu_2MnAl alloy was aged at temperatures ranging from 460℃ to 560℃, the morphology of the β-Mn precipitates would change with the different aging temperature; however, in spite of the morphology change the same orientation relationship between the β-Mn and the $L2_1$ matrix was maintained. This result is different from that reported by Kozubski et al. [4]. However, to date, all of the examinations were focused on the $Cu_{3-x}Mn_xAl$ alloys with $X \leqq 1.0$. Little information was available concerning the microstructural developments of the $Cu_{3-x}Mn_xAl$ alloys containing higher Mn content. Therefore, the purpose of this work is an attempt to study the phase transformations in the $Cu_{1.6}Mn_{1.4}Al$ alloy.

4-2 Experimental procedure

The alloy, $Cu_{1.6}Mn_{1.4}Al$ (Cu-35.1at.%Mn-25.1at.%Al), was prepared in a vacuum induction furnace by using 99.9 % Cu, 99.9 % Mn and 99.9 % Al. The melt was chill cast into a 30x50x200-mm-copper mold. After being homogenized at 900℃ for 72 hours, the ingot was sectioned into 2.0-mm thick slices. These slices were subsequently solution heat-treated at 900℃ for 1 hour and then quenched into room-temperature water rapidly. The aging process was performed at temperature ranging from 460℃ to 700℃ for various times in a vacuum heat-treated furnace and then quenched rapidly.

TEM specimens were prepared by means of a double-jet electropolisher with an electrolyte of 70% methanol and 30% nitric acid. The polishing temperature was kept in the range from -30℃ to -15℃, and the current density was kept in the range from $3.0x10^4$ to $4.0x10^4$ A/m^2. Electron microscopy was performed on a JEOL JEM-2000FX scanning transmission electron microscope operating at 200 KV. This microscope was equipped with a Link ISIS 300 energy-dispersive X-ray spectrometer (EDS) for chemical analysis. Quantitative analyses of elemental concentrations for Cu, Mn and Al were made with the aid of a Cliff-Lorimer Ratio Thin Section method.

4-3 Results

Figure 4.1(a) shows a bright-field (BF) electron micrograph of the as-quenched alloy. Figures 4.1(b) and (c) are two selected-area diffraction patterns (SADPs) of the as-quenched alloy. When compared with our previous studies in the $Cu_{2.2}Mn_{0.8}Al$ and Cu_2MnAl alloys [7-8], it is found in these SADPs that the brighter and well-arranged reflection spots are of the ordered $L2_1$ phase and the extra spots with streaks are of the L-J phase with two variants. Although the brighter and well-arranged reflection spots could be analyzed as a single $L2_1$ phase, the $L2_1$ reciprocal lattices contain all the B2-type reflections [9-10]. Therefore, in order to decide whether the ordered B2-type phase coexists with the $L2_1$ phase, both electron diffraction method and dark-field technique were performed. In our previous study [6], it was found that the intensity of the $(\bar{1}11)$ and (002) reflection spots of a single $L2_1$ phase should be almost equivalent. However, it is clearly seen in Figure 4.1(c) that the (002) and $(\bar{2}22)$ reflection spots are much stronger than the $(\bar{1}11)$ reflection spot. Therefore, it is strongly suggested that the (002) and $(\bar{2}22)$ reflection spots should derive from not only $L2_1$ phase but also the B2 phase, since the $(\bar{1}11)$ reflection spot comes from the $L2_1$ phase only; while the (002) and $(\bar{2}22)$ reflection spots can come from both the $L2_1$ and B2 phases (the (002) and $(\bar{2}22)$ $L2_1$ reflection spots are equal to the (001) and $(\bar{1}11)$ B2 reflection spots, respectively). Figures 4.1(d) and (e) are $(\bar{1}11)$ and (002) $L2_1$ dark-field (DF) electron micrographs of the as-quenched alloy. It is obviously seen that the bright region in the (002) DF image is much more

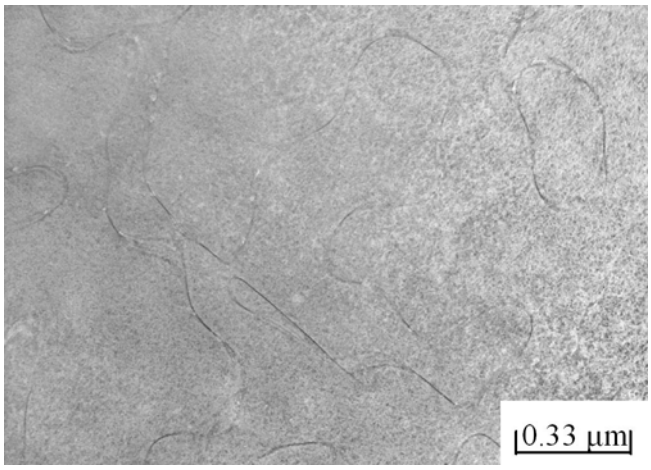

Figure 4.1 (a)

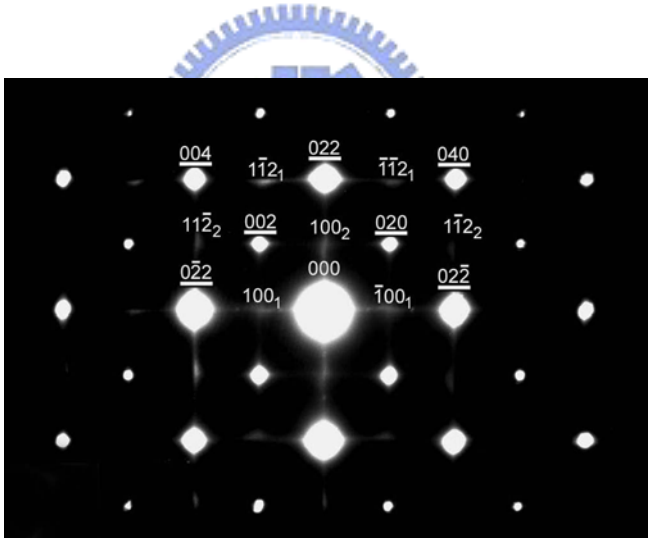

Figure 4.1 (b)

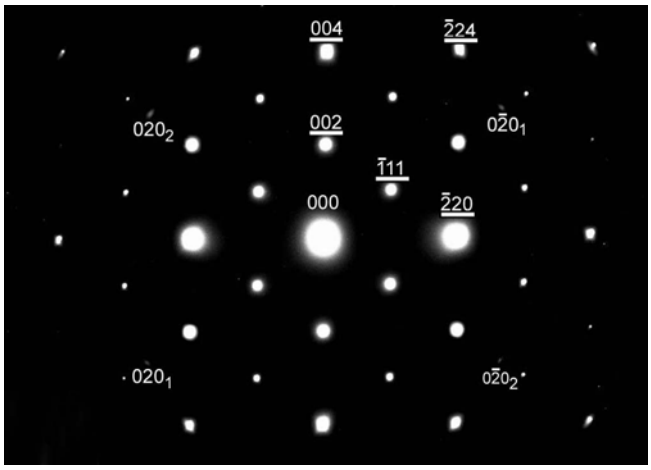

Figure 4.1 (c)

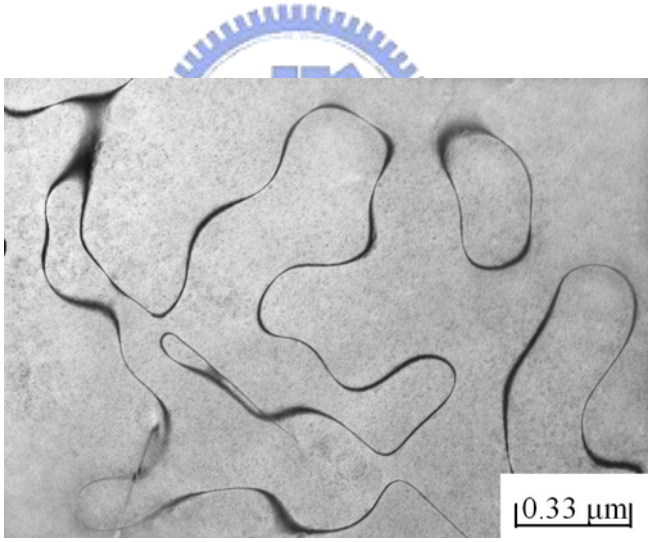

Figure 4.1 (d)

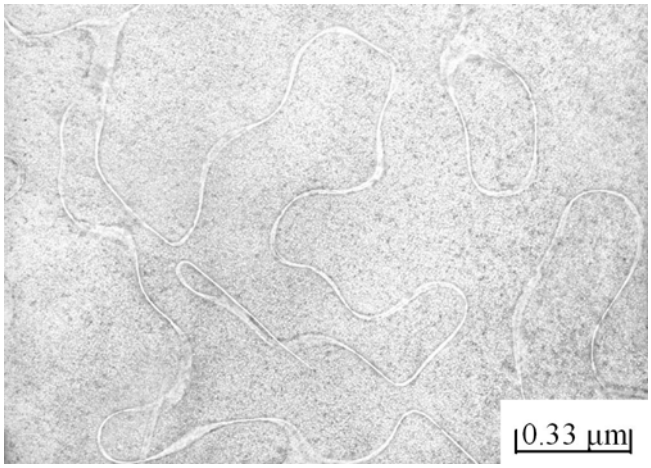

Figure 4.1 (e)

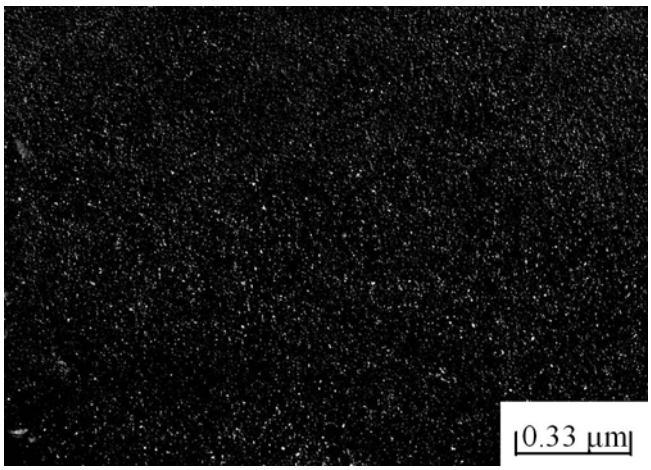

Figure 4.1 (f)

Figure 4.1 Electron micrographs of the as-quenched alloy. (a) BF, (b) through (c) two SADPs. The zone axes of the $L2_1$ phase are $[100]$ and $[110]$, respectively (<u>hkl</u>= $L2_1$, $hkl_{1,2}$= L-J phase, 1:variant 1; 2:variant 2). (d) and (e) $(\bar{1}11)$ and (002) $L2_1$ DF, respectively. (f) (100_1) L-J DF.

than that in the $(\bar{1}11)$ DF image. This demonstrates that both B2 and $L2_1$ phases are present, rather than single $L2_1$ phase; otherwise these two DF images should be morphologically identical. Figure 4.1 (f) is a (100_1) L-J DF electron micrograph, revealing the presence of fine L-J precipitates. Accordingly, it is concluded that the microstructure of the alloy in the as-quenched condition was a mixture of ($L2_1$ + B2 + L-J) phases.

When the as-quenched alloy was aged at 460℃ for less than 10 minutes, the sizes of both the B2 and L-J phases existing within the $L2_1$ matrix increased and the microstructure of the alloy was still the mixture of ($L2_1$ + B2 + L-J) phases. An example is shown in Figure 4.2. However, after prolonged aging at the same temperature, heterogeneous precipitation started to occur at the APBs, as illustrated in Figure 4.3(a). Figure 4.3(b) and (c) are two SADPs taken from an area including the precipitate marked as " r " in Figure 4.3(a) and its surrounding matrix. Based on the analyses of the diffraction pattern, it is confirmed that the heterogeneously precipitated phase is γ-brass and the orientation relationship between the γ-brass and the $L2_1$ matrix was determined to be cubic to cubic. This is similar to that reported by previous workers in the aged Cu_2MnAl alloy [4]. With continued aging at 460℃, the γ-brass precipitates grew and another type of precipitates started to occur at the regions contiguous to the γ-brass precipitates, as shown in Figure 4.4(a). Figures 4.4(b) and (c), two SADPs taken from the precipitate marked as "B" in Figure 4.4 (a), indicates that the new type of precipitate was β-Mn with lattice parameter a=0.641 nm [5-6, 8]. Figures 4.4(d) and (e) are two SADPs taken from the particle marked as "R" in Figure 4.4 (a), indicates that the particle

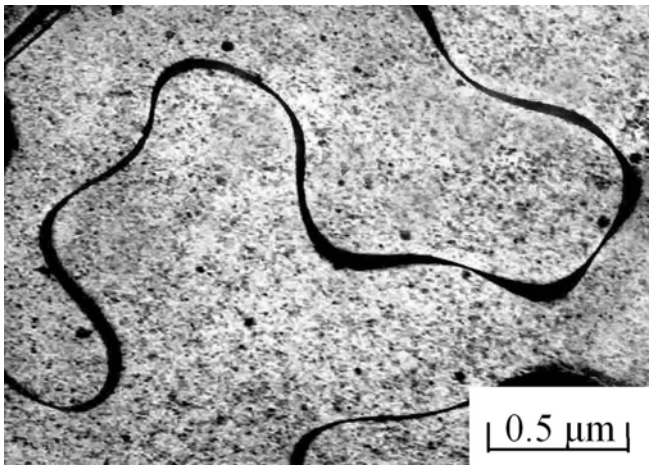

Figure 4.2 (a)

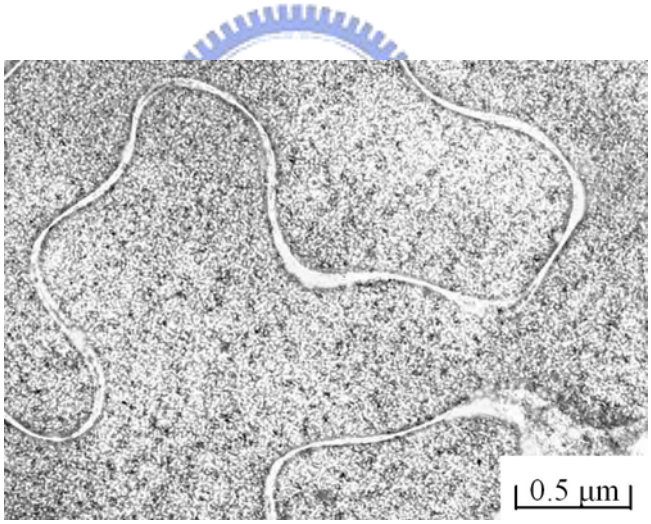

Figure 4.2 (b)

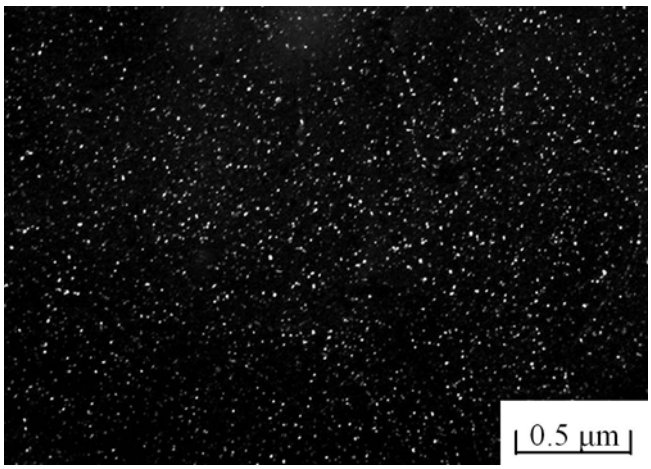

Figure 4.2 (c)

Figure 4.2 Electron micrographs of the alloy aged at 460℃ for 10 minutes. (a) and (b) ($\bar{1}11$) and (002) $L2_1$ DF, respectively. (c) (100_1) L-J DF.

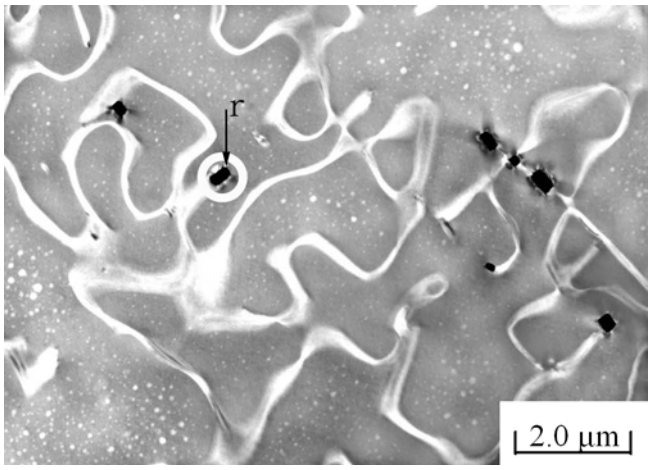

Figure 4.3 (a)

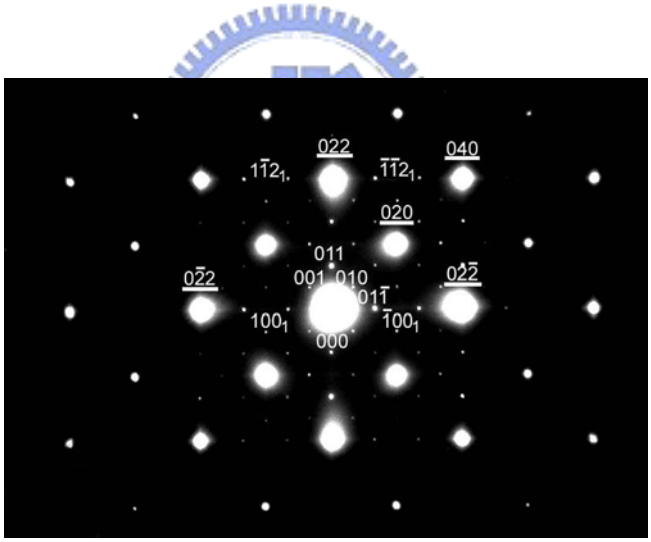

Figure 4.3 (b)

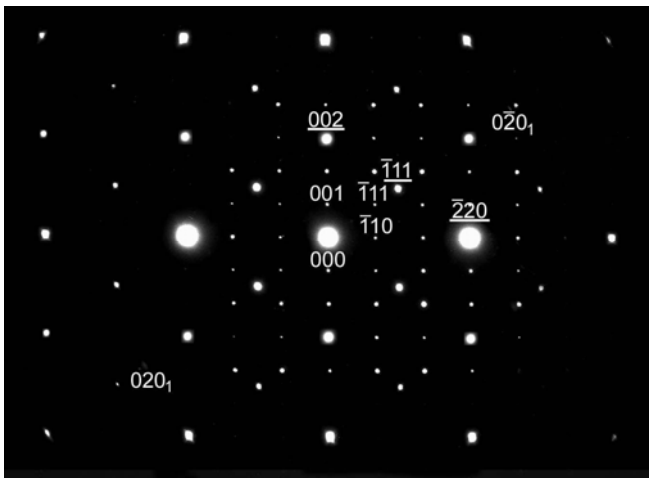

Figure 4.3 (c)

Figure 4.3 Electron micrographs of the alloy aged at 460℃ for 30 minutes. (a) (002) $L2_1$ DF, (b) and (c) two SADPs. The zone axes of the $L2_1$ phase is $[100]$ and $[110]$. (<u>hkl</u>= $L2_1$, hkl=γ-brass).

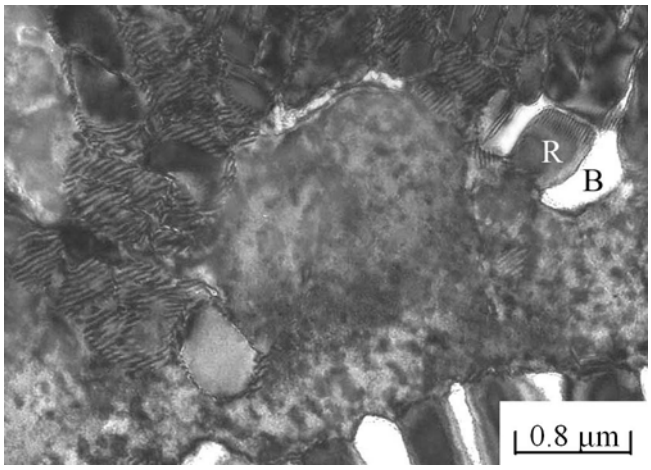

Figure 4.4 (a)

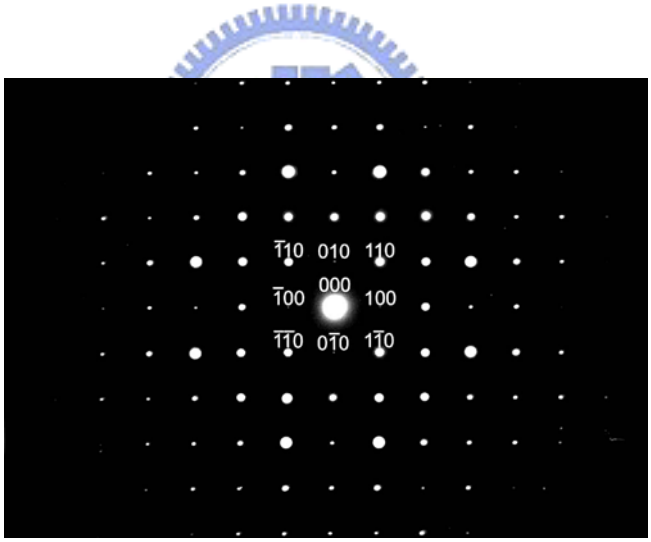

Figure 4.4 (b)

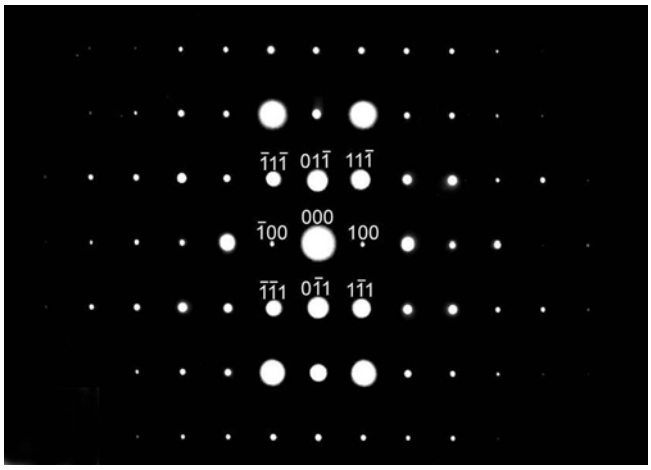

Figure 4.4 (c)

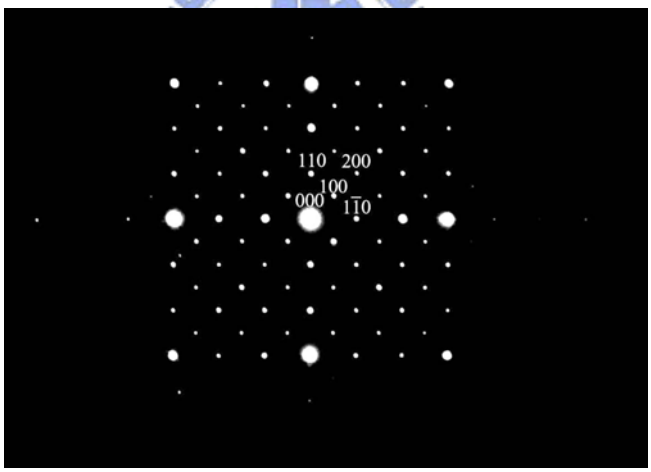

Figure 4.4 (d)

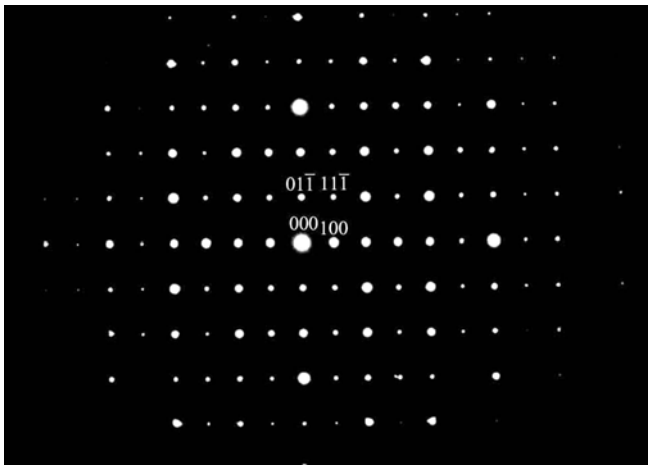

Figure 4.4 (e)

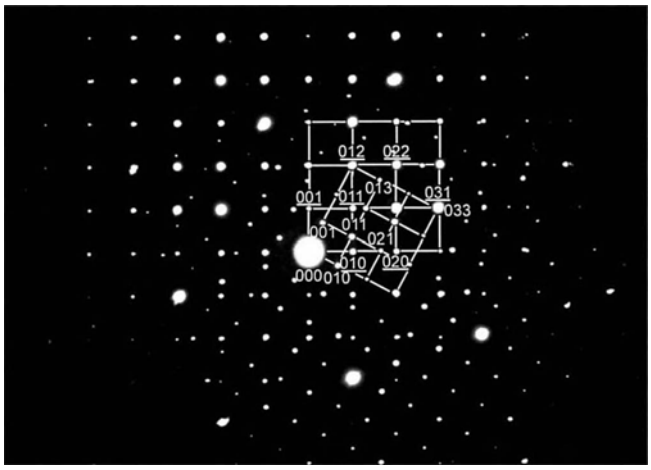

Figure 4.4 (f)

Figure 4.4 Electron micrographs of the alloy aged at 460°C for 6 hours. (a) BF, (b) and (c) two SADPs. The zone axes of the β-Mn are $[001]$ and $[011]$. (d) and (e) two SADPs. The zone axes of the γ-brass are $[001]$ and $[011]$. (f) an SADP. The zone axis of the β-Mn and the γ-brass is $[100]$ and $[100]$, respectively. (hkl=β-Mn, hkl=γ-brass).

was γ-brass phase. Figure 4.4(f) is an SADP taken from an area covering two precipitates marked as “R” and “B” in Figure 4.4(a), indicating that the orientation relationship between the γ-brass and β-Mn was $(001)_{\gamma\text{-brass}}$// $(012)_{\beta\text{-Mn}}$ and $(011)_{\gamma\text{-brass}}$//$(031)_{\beta\text{-Mn}}$. With the subsequent aging at 460℃, the precipitation of (γ-brass + β-Mn) would tend toward the inside of the $L2_1$ matrix, as illustrated in Figure 4.5. It is thus anticipated that the microstructure of the alloy in the equilibrium stage at 460℃ was a mixture of (γ-brass + β-Mn).

Transmission electron microscopy examinations revealed that the precipitates of (γ-brass + β-Mn) could exist up to 575℃. However, when the alloy was aged at 600℃, the mixture of (γ-brass + β-Mn) phases disappeared and some coarse precipitates with a granular shape occurred within the $L2_1$ matrix, as illustrated in Figure 4.6(a). Electron diffractions demonstrated that the coarse precipitates were the β-Mn phase. Figures 4.6(b) and (c) are two SADPs taken from the precipitate marked as “B” in Figure 4.6(a) and its surrounding $L2_1$ matrix. In these figures, indicate that the orientation relationship between the β-Mn and the $L2_1$ matrix is $(102)_{\beta\text{-Mn}}$ // $(001)_{L2_1}$, $(010)_{\beta\text{-Mn}}$ // $(010)_{L2_1}$ and $[20\bar{1}]_{\beta\text{-Mn}}$ // $[100]_{L2_1}$, $[100]_{\beta\text{-Mn}}$ // $[201]_{L2_1}$, which is similar to that found by the present workers in the Cu_2MnAl alloy [8]. Figures 4.6 (d) and (e) are $(\bar{1}11)$ and (002) $L2_1$ DF electron micrographs, clearly exhibiting small quenched-in $L2_1$ domains and the absence of a/4<111> APBs of B2 phase, respectively. Figure 4.6(f) is a (100_1) L-J DF electron micrograph. It is seen that the extremely fine L-J precipitates were formed during

quenching from the quenching temperature. This reveals that the microstructure of the alloy present at 600℃ was a mixture of (β-Mn + B2).

Progressively higher temperature aging and quenching experiments indicated that the β-Mn precipitates were preserved up to 675℃. However, when the alloy was aged at 700℃ and then quenched, the microstructure was similar to that observed in the as-quenched alloy, as shown in Figure 4.7.

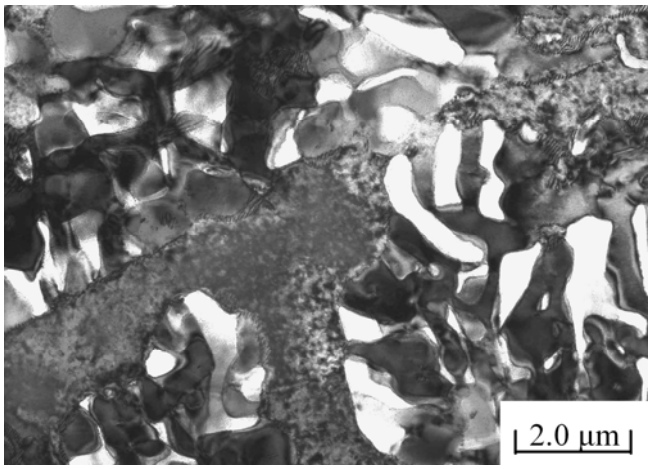

Figure 4.5

Figure 4.5 BF electron micrograph of the alloy aged at 460℃ for 12 hours.

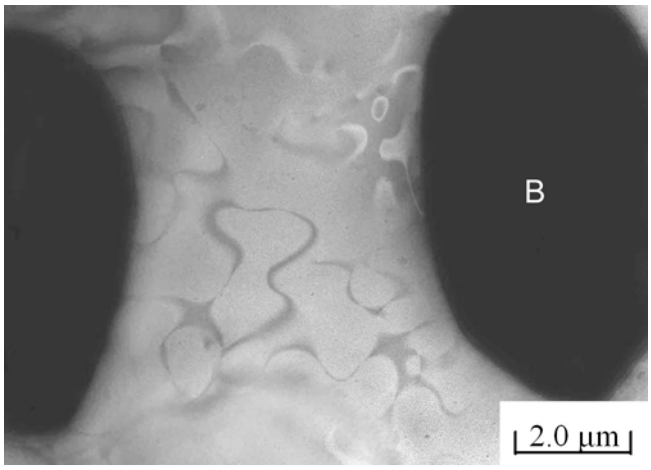

Figure 4.6 (a)

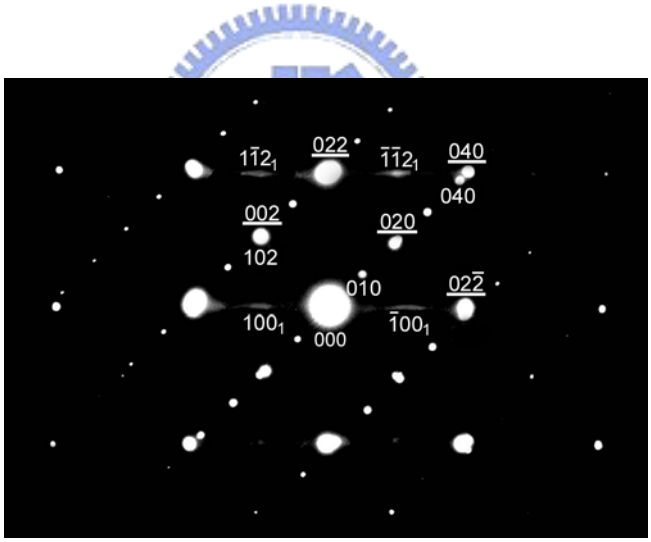

Figure 4.6 (b)

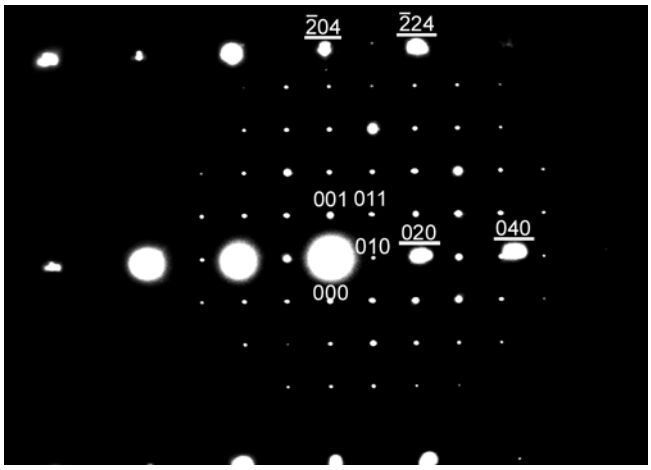

Figure 4.6 (c)

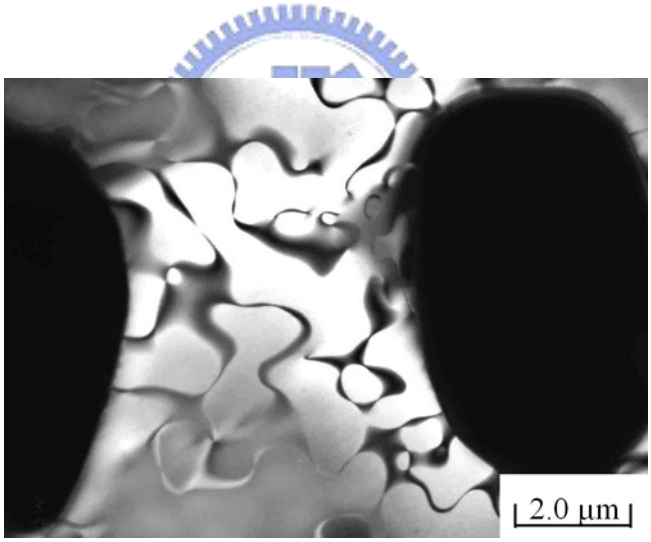

Figure 4.6 (d)

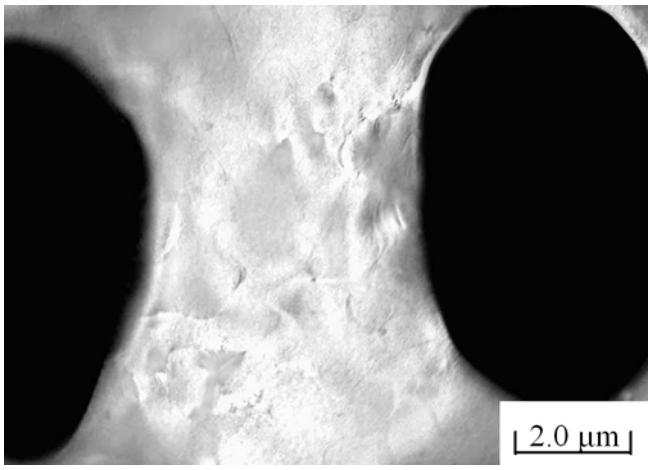

Figure 4.6 (e)

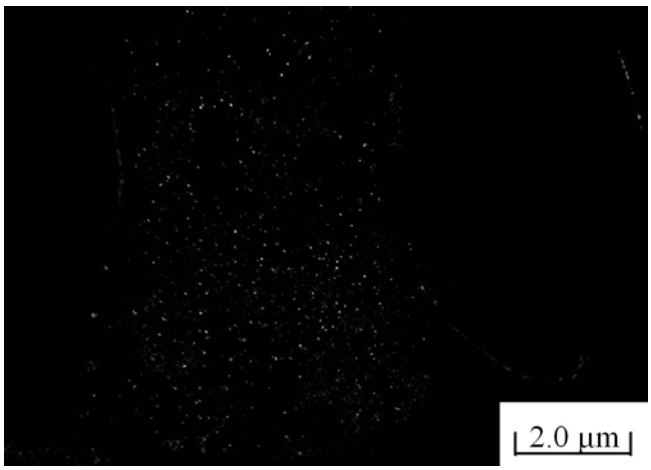

Figure 4.6 (f)

Figure 4.6 Electron micrographs of the alloy aged at 600℃ for 30 minutes. (a) BF, (b) and (c) two SADPs. The zone axes are $[20\bar{1}]_{\beta\text{–Mn}}$, $[100]_{\beta\text{-Mn}}$ for the β-Mn and $[100]_{L2_1}$, $[201]_{L2_1}$ for the $L2_1$ matrix, respectively. (<u>hkl</u>=β-Mn, hkl_1=L-J phase, hkl=γ-brass). (d) and (e) $(\bar{1}11)$ and (002) $L2_1$ DF, respectively. (f) (100_1) L-J DF.

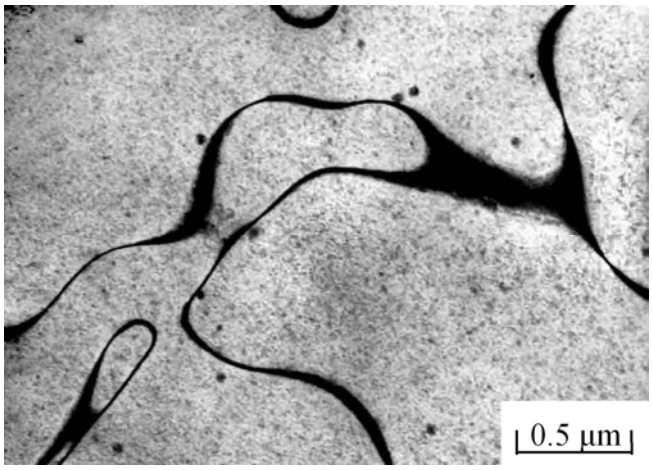

Figure 4.7 (a)

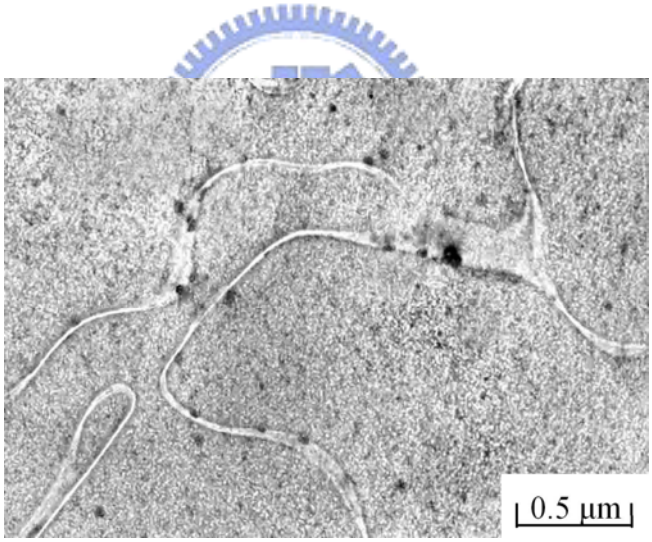

Figure 4.7 (b)

Figure 4.7 Electron micrographs of the alloy aged at 700℃ for 1 hour. (a) and (b) $(\bar{1}11)$ and (002) $L2_1$ DF, respectively.

4-4 Discussion

That the B2 phase could be detected in the as-quenched or aged at 460℃ alloy is a remarkable feature in the present study. This result is different from that examined by previous workers in the $Cu_{3-x}Mn_xAl$ alloys with $0.5 \leqq X \leqq 1.0$ [1-6], in which they reported that the as-quenched microstructure of the $Cu_{3-x}Mn_xAl$ alloys with $0.5 \leqq X \leqq 0.8$ was the ($D0_3$ + $L2_1$) phases, and that of the Cu_2MnAl alloy was the $L2_1$ phase; and the B2 phase could exist only at temperatures above 600℃. Compared to the previous studies [1-6], it is clear that besides containing higher Mn content, the chemical composition of the present alloy is similar to that of the $Cu_{3-x}Mn_xAl$ alloys with $0.5 \leqq X \leqq 1.0$. Therefore, it is reasonable to expect that the addition of the higher Mn content in the $Cu_{3-x}Mn_xAl$ alloys would pronouncedly enhance the formation of the B2 phase. However, the reason why the higher addition of Mn could lead to this result is unclear.

A second important feature of the present study is that when the alloy was aged at 460℃ for moderate times, the β-Mn precipitates started to occur at the regions contiguous to the γ-brass precipitates. This precipitation behavior has never been observed by previous workers in the aged Cu_2MnAl alloy [3-4], in which they found that when the Cu_2MnAl alloy was aged at temperatures ranging from 350℃ to 650℃, the γ-brass and β-Mn precipitates were formed separately at the grain boundaries or on other structural defects. In order to clarify this difference, an STEM-EDS study was undertaken. Figures 4.8(a) through (c) represent three typical EDS spectra taken from the

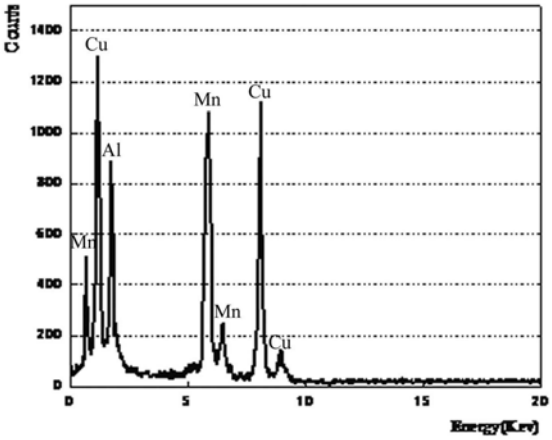

Figure 4.8 (a)

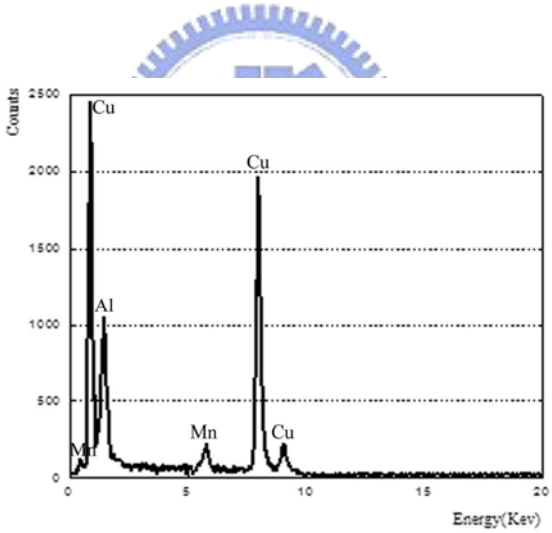

Figure 4.8(b)

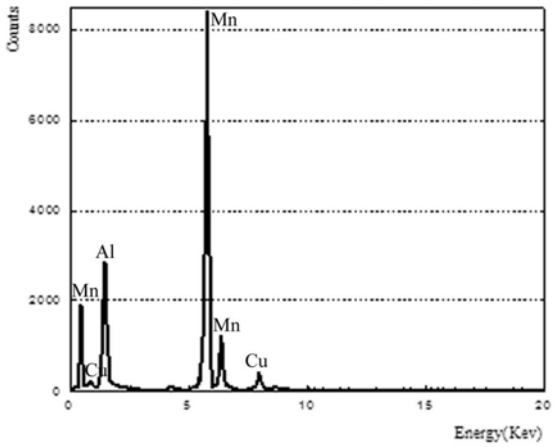

Figure 4.8 (c)

Figure 4.8 Three typical EDS spectra obtained from (a) as-quenched alloy, (b) a γ-brass precipitate as well as (c) a β-Mn precipitate in the alloy aged at 460℃ for 6 hours.

Table 4.1 Chemical Compositions of the Phases Revealed by an Energy-Dispersive X-ray Spectrometer (EDS)

Heat Treatment	Phase	Chemical Compositions (at.%)		
		Cu	Mn	Al
As-quenched	$L2_1$+B2+L-J	39.81	35.11	25.08
460℃, 6hrs	γ-brass	67.63	2.25	30.12
	β-Mn	11.99	67.97	20.04

as-quenched alloy and the γ-brass as well as the β-Mn precipitates in the alloy aged at 460℃ for 6 hours, respectively. The average concentrations of alloying elements obtained by analyzing a number of EDS spectra of each phase are listed in Table I. It is clearly seen in Table I that the concentration of Mn in the γ-brass is only about 2.25 at.%, which is much less than that in the as-quenched alloy. It is thus expected that along with the growth of the γ-brass precipitates, the surrounding regions would be enriched in Mn. In Cu-Mn phase diagram [11-12], it is clearly seen that the β-Mn phase could exist only when the Mn content was greater than 75 at.% and the temperature was in the range from 707℃ to 1100℃; whereas the β-Mn phase region was pronouncedly expanded to below 427℃ with 61 ≤ Mn ≤ 90 at.% and 10 ≤ Al ≤ 39 at.% in Al-Mn binary alloys [13-14]. Therefore, it is reasonable to propose that at lower temperature, the concentrations of both Al and Mn would be the predominant factor for the formation of the β-Mn precipitates. In Table I, it is obvious that the concentrations of both Al and Mn in the β-Mn precipitate are located within the composition range of the β-Mn phase region in the Al-Mn binary alloys. Therefore, the coexistence of (γ-brass + β-Mn) is expected to occur. In contrast to the observations in the present alloy, although the Mn-lack γ-brass precipitates were also observed to occur in the aged Cu_2MnAl alloy, no evidence of the β-Mn precipitates could be detected at the regions contiguous to the γ-brass precipitates [4, 8]. The reason is probably that along with the growth of γ-brass precipitates, the Mn concentration at the regions surrounding the γ-brass may not be sufficient to cause the formation of the β-Mn precipitates.

Finally, it is worthwhile to note that during the early stage of isothermal aging at 460℃, the γ-brass precipitates have occurred preferentially at APBs. This feature is similar to that observed by other workers in an aged Cu-4.6wt.%Al-4.1wt.%Ni alloy [15].

4-5 Conclusion

The phase transformations in the $Cu_{1.6}Mn_{1.4}Al$ alloy have been studied by using transmission electron microscopy and energy–dispersive X-ray spectrometry.

1. The as-quenched microstructure of the $Cu_{1.6}Mn_{1.4}Al$ alloy was a mixture of ($L2_1$ + B2 + L-J) phases, where the L-J phase and the fine B2 precipitates were formed within the $L2_1$ domains during quenching.

2. When the as-quenched alloy was aged at 460℃ for moderate times, β-Mn precipitates were formed at the regions contiguous to the γ-brass precipitates. The orientation relationship between the γ-brass and β-Mn was $(001)_{\gamma\text{-brass}}$ // $(012)_{\beta\text{-Mn}}$ and $(011)_{\gamma\text{-brass}}$ // $(031)_{\beta\text{-Mn}}$. The coexistence of (γ-brass + β-Mn) has never been observed by previous workers in Cu-Mn-Al alloy systems before.

3. When the as-quenched alloy was aged at 600℃, the β-Mn precipitates with a granular shape could be observed within the $L2_1$ matrix. The orientation relationship between the β-Mn and the $L2_1$ matrix is $(102)_{\beta\text{-Mn}}$ // $(001)_{L2_1}$, $(010)_{\beta\text{-Mn}}$ // $(010)_{L2_1}$ and $[20\bar{1}]_{\beta\text{-Mn}}$ // $[100]_{L2_1}$, $[100]_{\beta\text{-Mn}}$ // $[201]_{L2_1}$, which is similar to that found by the present workers in the

Cu_2MnAl alloy.

4. The phase transition sequence as the aging temperature increased from 460℃ to 700℃ was found to be (γ-brass + β-Mn) → (β-Mn + B2) → β.

References

1. M. Bouchard, G. Thomas: Acta Matall. 23 (1975) 1485.
2. R. Kainuma, N. Satoh, X.J. Liu, I. Ohnuma, K. Ishida: J. Alloy. Compd. 266 (1998) 191.
3. R. Kozubski, J. Soltys: J. Mater. Sci. 18 (1983) 1689.
4. R. Kozubski, J. Soltys, J. Dutkiewicz, J. Morgiel: J. Mater. Sci. 22 (1987) 3843.
5. B. Dubois, D. Chevereau: J. Mater. Sci. 14 (1979) 2296.
6. R. Kozubski. J. Solty: J. Mater. Sci. 17 (1982) 1441.
7. S.C. Jeng, T.F. Liu: Metall. Mater. Trans. 26A (1995) 1353.
8. K.C. Chu, T.F. Liu: Metall. Mater. Trans. 30A (1999) 1705.
9. T.F. Liu, G.C. Uen, C.Y. Chao, Y.L. Lin, C.C. Wu: Metall. Trans. 22A (1991) 1407.
10. C.C. Wu, J.S. Chou, T.F. Liu: Metall. Trans. 22A (1991) 2265.
11. F.A. Shunk, in: Thaddeus B. Massalski (ed.), Binary Alloy Phase Diagrams, American Society for Metals, Metals Park, Ohio, 1990, pp.1435.
12. K. Lewin, D. Sichen, S. Seetharaman: Scand. J. Metall. 22 (1993) 310.
13. X.J. Liu, I. Ohnuma, R. Kainuma, K. Ishida: J. Phase Equilib. 20 (1999) 45.
14. A.j. McAlster, J.L. Murray, Binary Alloy Phase Diagrams, 2nd ed., T.B. Massalski, P.R. Subramanian, H. okamoto, L. Kacprezak, Ed., ASM International, 1990, pp. 171.

15. N. Zárubová, A. Gemperle, V. Novák: Mater. Sci. Eng. A 222 (1997) 166.

Chapter 5.

Summary

Effects of the manganese content on the microstructural changes of the Cu-Mn-Al alloy systems have been examined. Based On these experimental results, some conclusions are given as follows:

1. In the as-quenched condition, the $D0_3$ phase in the $Cu_{3-x}Mn_xAl$ alloys with X ≤ 0.3 (Mn ≤ 7.5 at.%) was formed by a β → B2 → $D0_3$ ordering transition during quenching, However, a β → B2 → ($D0_3$ + $L2_1$) transition instead of the β → B2 → $D0_3$ was found to occur in the $Cu_{2.6}Mn_{0.4}Al$ (Mn=10.3 at.%) alloy. It is concluded that when the β phase of the $Cu_{3-x}Mn_xAl$ alloy systems with the Mn content less than 7.5 at.% didn't pass through a miscibility gap during quenching, so that only $D0_3$ phase could be observed in the as-quenched microstructure. No $L2_1$ phase could be detected at this moment.

2. The a/4<111> (APBs) could be clearly observed in the $Cu_{3-x}Mn_xAl$ alloys with X ≤ 0.3. However, no evidence of the a/4<111> APBs could be detected in the $Cu_{3-x}Mn_xAl$ alloys with X ≥ 0.4. This result seems to imply that the increase of the manganese content in the Cu-Mn-Al alloys could decrease the a/4<111> APBs energy. Therefore, this may be one possible reason to account for the absence of the a/4<111> APBs in the previous studies of the as-quenched $Cu_{3-x}Mn_xAl$ alloys with $0.5 \leqq X \leqq 1.0$.

3. The sizes of both B2 and $D0_3$ domains increased with increasing Mn content. This implies that an increase of the Mn content would increase A2

→B2 and the B2 → $D0_3$ ordering transition temperature. In addition, the amount of the L-J phase increased with increasing the Mn content, too. It seems to imply that the higher Mn content in the $Cu_{3-x}Mn_xAl$ alloys may enhance the formation of the extremely fine L-J precipitates within the matrix during quenching.

4. The as-quenched microstructure of the $Cu_{2.7}Mn_{0.3}Al$ (Cu-7.6at.%Mn -25.1at.%Al) alloy was $D0_3$ phase containing extremely fine L-J precipitates. When the as-quenched alloy was aged at temperatures ranging from 500℃ to 700℃, the phase transition sequence was found to be (γ-brass + L-J + $D0_3$) → (γ-brass + L-J + B2) → β, rather than (γ-brass + $D0_3$) → (γ-brass + B2) → β reported by previous workers in $Cu_{3-x}Mn_xAl$ alloys with X ≤ 0.32. The coexistence of (γ-brass + L-J) phases has never been observed by other workers in the Cu-Mn-Al alloy systems before.

5. The as-quenched microstructure of the $Cu_{1.6}Mn_{1.4}Al$ (Cu-35.1at.%Mn -25.1at.%Al) alloy was a mixture of ($L2_1$ + B2 + L-J) phases, where the L-J phase and the fine B2 precipitates were formed within the $L2_1$ domains during quenching. When the as-quenched alloy was aged at 460℃ for moderate times, β-Mn precipitates were formed at the regions contiguous to the γ-brass precipitates. The orientation relationship between the γ-brass and β-Mn was $(001)_{\gamma\text{-brass}}$ // $(012)_{\beta\text{-Mn}}$ and $(011)_{\gamma\text{-brass}}$ // $(031)_{\beta\text{-Mn}}$. The coexistence of (γ-brass + β-Mn) has never been

observed by other workers in Cu-Mn-Al alloy systems before. The phase transition sequence as the aging temperature increased from 460℃ to 700℃ was found to be (γ-brass + β-Mn) → (β-Mn + B2) → β.

List of Publications

- Journal Papers

1. S.Y. Yang and T.F. Liu, “As-quenched Microstructures of Cu_{3-x} Mn_xAl Alloys”, accepted for publication in Mater. Chem. Phys. (2005,9)
2. S.Y. Yang and T.F. Liu, “Phase transformations in a Cu-25 at.% Al-7.5at.%Mn Alloy”, accepted for publication in Scripta Mater. (2005,10)
3. S.Y. Yang and T.F. Liu, “Phase transformations in a Cu-25at.% Al-35at.%Mn Alloy”, accepted for publication in J. Alloy. Compd. (2005,9)

- Conferences Papers

1. S.Y. Yang, J.S. Weng , S.C. Jeng, P.T. Kuo and T.F.Liu, “As-quenched Microstructures of $Cu_{3-x}Mn_xAl$(X=0.1, 0.2, 0.3 and 0.4) Alloys”, Proceedings of The 2005 Annual Conference of The Chinese Society for Materials Science 1-2-P-022 (2005)
2. S.Y. Yang, I.M. Peng, J.S. Weng and T.F.Liu, “Phase Transformations in an $Cu_{2.75}Mn_{0.25}Al$ Alloy Alloy”, Proceedings of The 2004 Annual Conference of The Chinese Society for Materials Science PA2-064 (2004)
3. J.W. Lee, S.Y. Yang, C.B. Ho and T.F. Liu, “Phase Transformations in an

Fe-9Al-30Mn-5Cr-1.2Si Alloy", Proceedings of The 2003 Annual Conference of The Chinese Society for Materials Science PA-031 (2003)

4. 李堅瑋, 林敻松, 楊勝裕, 彭英銘, 劉增豐 "退火熱處理對熱浸鍍鋁鐵鋁錳碳合金鍍層的影響之研究", Proceedings of The 2003 Annual Conference of The Chinese Society for Materials Science PA-032 (2003)
5. C.H. Chen, S.Y. Yang, J.X. Lin and T.F. Liu, "Phase Transformations in a Cu-14.5Al-9.0Ni Alloy", Proceedings of The 2002 Annual Conference of The Chinese Society for Materials Science, B-34 (2002)
6. C.H. Chen, J. Tan, C.P. Wang, C.S. Wang, S.Y. Yang, and T.F. Liu, "Phase Transformations in a Cu-14.2Al-10.0Ni Alloy", Proceedings of The 2000 Annual Conference of The Chinese Society for Materials Science, B-11 (2000)
7. S.Y. Yang, C.P. Wang, C.H. Chen, C.S. Wang, J.W. Lee, and T.F. Liu, "Phase Transformations in an Fe-8.8Al-30.0Mn-6.0Mo-1.1 C Alloy", Proceedings of The 2000 Annual Conference of The Chinese Society for Materials Science, A-25 (2000)
8. C.S. Wang, I.S. Lo, C.P. Wang, C.H. Chen, S.Y. Yang, and T.F. Liu, "Phase Transformations in an Fe-8.8Al-30Mn-6Cr-1C Alloy", Proceedings of The 2000 Annual Conference of The Chinese Society for Materials Science, A-27 (2000)

9. C.P. Wang, Q.W. Yang, C.S. Wang, C.H. Chen, S.Y. Yang, J.W. Lee, and T.F. Liu, "Phase Transformations in an Fe-8Al-12Ni-2C Alloy", Proceedings of The 2000 Annual Conference of The Chinese Society for Materials Science, A-26 (2000)